Recoil-decay tagging study of ^{205}Fr

U. Jakobsson,[1,*] J. Uusitalo,[1] S. Juutinen,[1] M. Leino,[1] T. Enqvist,[2] P. T. Greenlees,[1] K. Hauschild,[1,3] P. Jones,[1,†] R. Julin,[1] S. Ketelhut,[1,‡] P. Kuusiniemi,[2] M. Nyman,[1] P. Peura,[1] P. Rahkila,[1] P. Ruotsalainen,[1] J. Sarén,[1] C. Scholey,[1] and J. Sorri[1]

[1]*Department of Physics, University of Jyväskylä, P. O. Box 35, FI-40014 Jyväskylä, Finland*

[2]*Oulu Southern Institute and Department of Physics, University of Oulu, FI-90041 Oulu, Finland*

[3]*CSNSM, IN2P3-CNRS, F-91405 Orsay Campus, France*

(Received 1 October 2011; published 12 January 2012)

The nucleus ^{205}Fr has been studied through γ-ray and electron spectroscopy using the recoil-decay tagging technique. The resulting level scheme presents a spherical structure built on the $9/2^-$ ground state and a rotational structure on top of a short-lived isomer. The isomer, with a spin and parity of $13/2^+$ and a half-life of 80(20) ns, de-excites by an $M2$ transition directly to the $9/2^-$ ground state. Another, longer-lived, isomer, with a half-life of 1.15(4) ms, has also been found and assigned a spin and parity of $1/2^+$. Transitions populating and de-exciting this isomer have been observed as well.

DOI: 10.1103/PhysRevC.85.014309 PACS number(s): 23.20.Lv, 23.35.+g, 27.80.+w, 29.30.Kv

I. INTRODUCTION

Shape coexistence has been studied throughout neutron-deficient nuclei in the lead region. A competition among spherical, oblate, and prolate shapes has been reported to exist in nuclei up to $Z = 84$ (see Ref. [1] and references therein). The gradual transition between spherical and deformed shapes is believed to be caused by the increasing number of neutron holes, when approaching the neutron mid-shell, coupling to the particle-hole excitations across the proton shell gap. This interaction is attractive and, thus, brings the resulting nuclear states down in energy and increases the collective behavior. The major challenge in studying these proton drip-line nuclei is the decreasing production yield due to the increase of fission.

An onset of oblate ground-state deformation, associated with the 2p-2h excitation across the proton shell gap, has been reported to occur in even-mass polonium nuclei around $N \leqslant 114$ [2–4]. Low-lying excited states in neutron-deficient radon nuclei have been studied down to ^{198}Rn [5–10]. An increase in collectivity for these states, caused by the increasing number of neutron-hole pairs is reported, showing signs of contributions from the 2p-2h excitation. α-decay properties obtained for ^{193}Rn [11] and ^{196}Rn [12] suggest an onset of oblate ground-state deformation in ^{196}Rn and, further, of prolate deformation in ^{193}Rn. The chain of corresponding neutron-deficient odd-mass francium nuclei is less well known than the radon isotopes, with ^{205}Fr being the lightest isotope with in-beam studies reported to date [13–15]. No onset of deformation has been observed in these nuclei.

The $1/2^+$ state, created by exciting a proton from the $s_{1/2}$ shell across the proton shell gap, is well known throughout the odd-mass bismuth nuclei. The state is highly nonyrast in ^{199}Bi and ^{201}Bi [16]. It comes down in energy with decreasing neutron number and becomes the ground state in ^{185}Bi [17]. Interesting features have been observed related to this state throughout the isotopic chain, such as very slow $M4$ transitions to the $9/2^-$ ground state [16]. In the astatine nuclei the state is first observed in ^{197}At [18], decaying by α emission, and it becomes the ground state in ^{195}At [19]. Uusitalo *et al.* [20] have observed the $1/2^+$ state in ^{203}Fr and ^{201}Fr through α-decay studies. In ^{201}Fr the level lies at 146 keV, but in ^{203}Fr the level energy has not yet been established, as the corresponding state in the α-decay daughter ^{199}At has also not been observed. The $1/2^+$ state is expected to become the ground state in ^{199}Fr, leading to oblate ground-state deformation [20].

Another state, characteristic of this region, is the $13/2^+$ state based on the odd proton excited to the $i_{13/2}$ shell. Throughout the odd-mass bismuth and astatine nuclei this state is better known than the $1/2^+$ state. For instance, when approaching the neutron mid-shell, the $13/2^+$ state first becomes isomeric in ^{201}At [21], yrast in ^{199}At, and α decaying in ^{193}At [22]. In ^{199}At and ^{197}At rotational bands have been observed to be built on the $13/2^+$ state, with an estimated deformation parameter of $\beta_2 = -0.2$ in ^{197}At [18]. The $13/2^+$ state has not yet been observed in the odd-mass francium nuclei with $A < 213$.

The nucleus ^{205}Fr has previously been reported by Hartley *et al.* [15], presenting a level scheme with tentative spin and parity assignments constructed up to nearly $10\hbar$ with a level energy of 1736 keV. The transitions were associated with a francium nucleus based on the x rays visible in the coincidence data and, further, with the nucleus ^{205}Fr by total γ-ray fold distributions and cross-bombardment. The assignment of this structure was supported by its similarity with the structure of the one assigned for ^{207}Fr [15].

The present work investigates the possible shape coexistence in ^{205}Fr. Isomeric states generated by the $i_{13/2}$ and the intruding $s_{1/2}$ orbitals are presented, with excited states built on these isomers. Transitions to the ground state are also presented. The present work disagrees entirely with the previous study presented by Hartley *et al.* on the excited states in ^{205}Fr. This disagreement will be discussed as well.

*ulrika.jakobsson@jyu.fi

†Present address: iThemba Laboratory for Accelerator Based Sciences, P. O. Box 722, 7129 Somerset West, South Africa.

‡Present address: TRIUMF, Westbrook Mall, Vancouver, British Columbia, V6T 2A3 Canada.

II. EXPERIMENTAL DETAILS

The measurements were conducted in the Accelerator Laboratory at the Department of Physics of the University of Jyväskylä (JYFL), Finland. The nucleus ^{205}Fr was produced in the fusion-evaporation reaction ^{169}Tm(^{40}Ar, $4n$)^{205}Fr. The ^{40}Ar ion beam, provided by the K-130 cyclotron, was accelerated to an energy of 180 MeV with an average beam current of 14 particle-nA (pnA), during an irradiation time of 60 h. The self-supporting ^{169}Tm target had a thickness of 410 μg/cm^2, and a 50-μg/cm^2-thick carbon reset foil was used behind the target. The ^{205}Fr isotopes were produced with a cross section of 1.3 mb. The rate of detected fusion-evaporation products was estimated to be 27 Hz.

The JUROGAM Ge-detector array was used to detect prompt γ rays at the target position. The array consisted of 43 Compton-suppressed high-purity germanium (HPGe) detectors of EUROGAM phase one [23] and GASP [24] type. The recoiling fusion-evaporation products were separated from beam particles and other unwanted reaction products by the gas-filled recoil separator RITU [25] and transported to the GREAT spectrometer [26] at its focal plane. When arriving in GREAT, the recoils passed through a multiwire proportional counter (MWPC) and were finally implanted into a 300-μm-thick double-sided silicon strip detector (DSSD), which has 4800 pixels in total. The horizontal strips of the DSSD were set to measure α-decay energies and the vertical strips to measure conversion-electron energies, by adjusting the gain ranges of the amplifiers. A clover and a planar germanium detector were used to detect delayed γ rays close to the DSSD, and a silicon PIN-detector array, situated upstream in a box arrangement at the edges of the DSSD, was used for detecting conversion electrons. The PIN detectors and the vertical strips of the DSSD were calibrated using a ^{133}Ba source. All data channels were recorded synchronously using the triggerless total data readout (TDR) [27] data acquisition system, which gives each event an absolute time stamp with a time resolution of 10 ns.

III. RESULTS

The measurement data were analyzed using the recoil-decay tagging (RDT) technique [28] and processed using the GRAIN [29] and RADWARE [30,31] software packages. The recoiling fusion-evaporation products were selected by their time of flight between the MWPC and the DSSD and their energy loss in the MWPC. Furthermore, the different isotopes were identified by linking the recoils with their subsequent α decays in the DSSD, using spatial and temporal correlations. The α-decay branch of $\geqslant$98.5% [32] and half-life of 3.80(3) s [33] for the $9/2^-$ ground state allowed for an effective identification of the ^{205}Fr recoils using a maximum correlation time of 12 s between the recoil and its subsequent α decay. The MWPC-vetoed α-particle energy spectrum obtained from the ^{40}Ar + ^{169}Tm reaction is shown in Fig. 1. Prompt and delayed γ rays belonging to ^{205}Fr were identified based on their time correlation with the α-tagged recoil observed in the DSSD.

The delayed γ-ray and electron spectra in Fig. 2 are collected from recoil-correlated events detected in the GREAT clover detector and the PIN-detector array, respectively. The 440-keV peak in the electron spectrum represents the K-shell conversion of the 544-keV isomeric transition. An internal K-shell conversion coefficient of 0.25(10) can be obtained by comparing the intensities of the peaks in the two spectra (simulated efficiencies were used for the PIN-detector array; see Ref. [34]). This result suggests an $M2$ multipolarity for the isomeric transition [35]. The half-life of the isomer could not be directly determined, due to poor statistics. Based on the feeding of the isomer detected in the JUROGAM array, the number of events detected in the GREAT clover detector and the flight time of the recoil through RITU, a value of 80(20) ns can be estimated for the half-life of the isomer. The estimates assume roughly equal efficiencies for the JUROGAM array and the GREAT clover detector

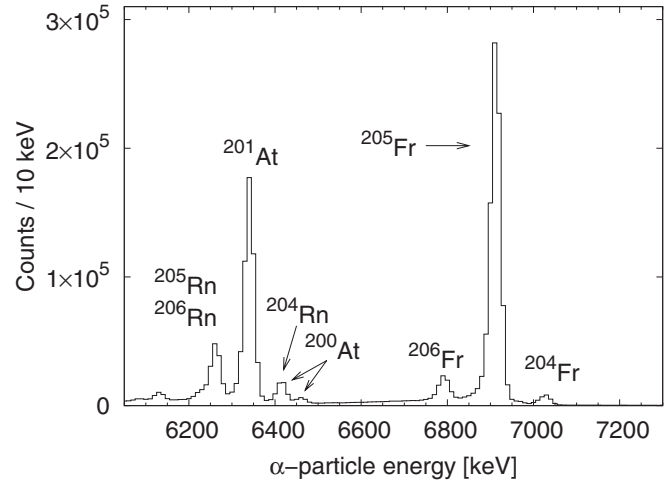

FIG. 1. The MWPC-vetoed α-particle energy spectrum obtained using the ^{40}Ar + ^{169}Tm reaction.

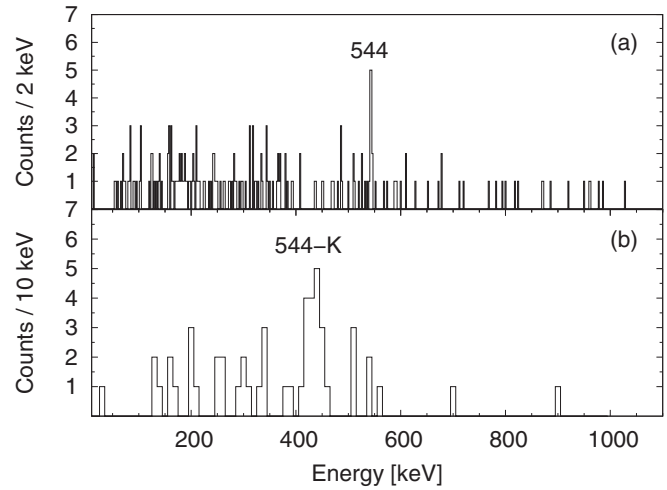

FIG. 2. (a) The spectrum of the delayed γ rays detected in the GREAT clover detector, associated with a recoil implantation in the DSSD. (b) The corresponding conversion electrons detected in the PIN-detector array. A correlation time of 100 ns was used between the recoil implantation and the isomeric decay to get optimal visibility of the peaks.

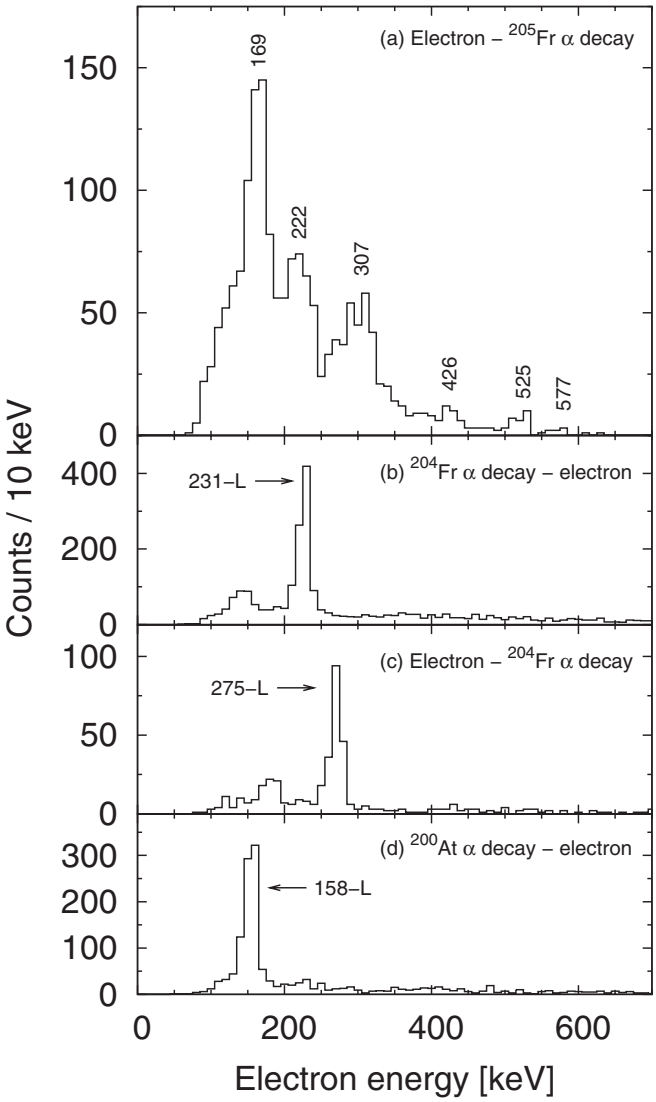

FIG. 3. Energy spectra of electrons detected in the horizontal strips of the DSSD. (a) The spectrum obtained by tagging with the ^{205}Fr α decay, using a correlation time of 8 ms between the recoil and the isomeric decay. The spectrum consists of events from a cascade of electrons. [(b)–(d)] The conversion-electron spectra obtained by tagging with the α decays of ^{204}Fr and ^{200}At [38], using a correlation time of 5 s between the α decay and the subsequent electron in panel (b), 3 s between the recoil implantation and the electron in panel (c), and 5 s between the α decay and the subsequent electron in panel (d). See text for further details.

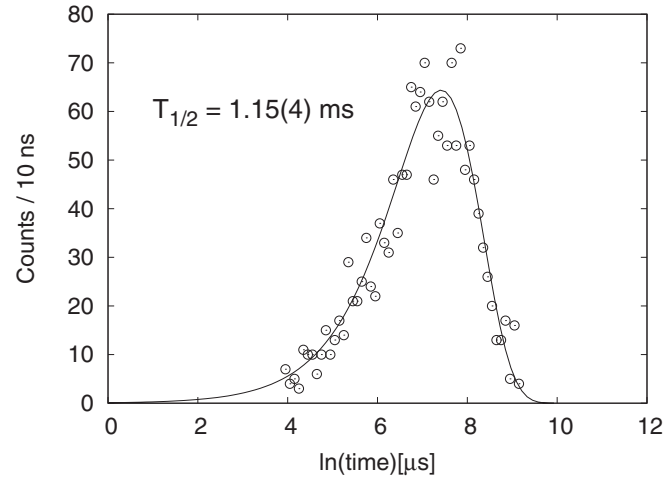

FIG. 4. Time distribution between ^{205}Fr recoil implantation and the subsequent de-excitation of the $1/2^+$ isomer detected in the PIN-detector array. See Ref. [40] for method details. A time window between 50 μs and 8 ms was used, with the lower limit set to eliminate noise effects.

[34]. Based on the results obtained, a transition strength of 0.17(4) W.u. was determined for this $M2$ transition. This value is comparable with those obtained for $M2$ transitions depopulating the $13/2^+$ isomer directly to the $9/2^-$ ground state in odd-mass astatine nuclei. For example, the values 0.182(22) W.u. for ^{201}At [36], 0.16(5) W.u. for ^{199}At [37], and 0.086(13) W.u. for ^{197}At [18] have been reported. Based on these observations the spin and parity of the fast isomer is assigned to be $13/2^+$.

Another, longer-living, isomeric state was also observed by studying ^{205}Fr α-tagged delayed electrons and γ-ray transitions detected in the GREAT DSSD and the planar and clover detectors, respectively. A correlation time of 8 ms was used between the implantation of the ^{205}Fr recoil and the detection of the isomeric decay. Figure 3(a) presents the ^{205}Fr α-tagged electrons with internal-conversion electron spectra [Figs. 3(b)–3(d)] related to the α decays of ^{204}Fr and the daughter nucleus ^{200}At [38,39]; see Fig. 1. Figure 3(b) presents the 231-keV $E3$ transition from the 10^- state in ^{200}At following the 7013-keV α decay of ^{204}Fr, Fig. 3(c) the 275-keV $E3$ transition from the 10^- state in ^{204}Fr preceding the 6969-keV α decay (this transition is now observed, while previous results obtained the transition energy from the difference of the α-decay energies), and Fig. 3(d) the 158-keV $M3$ transition from the 6^+ state in ^{196}Bi following the 6411-keV α decay of ^{200}At. The spectra in Figs. 3(b) and 3(d) provide a means for internal calibration of the spectrum in Fig. 3(a). It is worth noting that since the FWHM is close to 12 keV for the obtained electron peaks, the L- and higher shell conversion electrons will not be separated, and a sum peak representing all these events should situate roughly 12–13 keV below the corresponding transition energy. In this special case, the internal conversion takes place inside the DSSD. Therefore, the energy deposited by the Auger electrons and low-energy x rays, released in the internal conversion process, sum up with the energy deposit of the conversion electron, giving an additional ~10 keV to the total energy deposit. As a result, the electron peak representing emission from the $L + M$ (+higher) shells is found close to 2–3 keV below the corresponding transition energy. This effect is also confirmed in simulations performed for the cases presented above.

Figure 4 presents the time difference between the recoil implantation and the electrons in Fig. 3(a). Using the logarithmic-time method [40] a half-life of 1.15(4) ms was obtained for the isomeric decay. Based on the half-life the assumption can be made that the longer living isomer is actually the $1/2^+$ isomer. Figure 5 depicts the spectrum of delayed

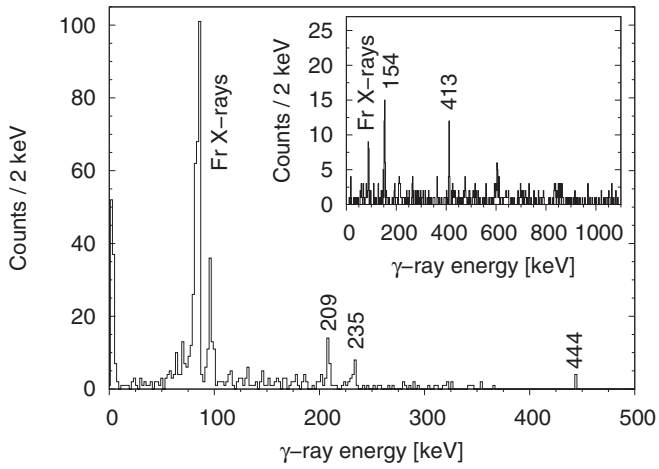

FIG. 5. Spectrum of delayed γ rays tagged with the ^{205}Fr α decay, detected in the GREAT planar and clover detector, in coincidence with electrons associated with the 1.15(4)-ms isomer. (Inset) The spectrum of prompt γ rays detected in the JUROGAM array and associated with the isomeric decay. A correlation time of 8 ms was used between the recoil implantation and the isomeric decay. Note the broad peaks close to 600 and 840 keV originated from the $(n, n'\gamma)$ reaction in the detector material.

γ rays obtained from the GREAT planar and clover detector tagged with the isomeric electrons in Fig. 3(a). Two γ-ray transitions with energies of 209 and 235 keV are clearly visible together with a weaker 444-keV peak. To understand the complicated structure of the electron spectrum in Fig. 3(a), the 209- and 235-keV transitions need to be in a cascade with an additional highly converted ($M2$ or $E3$) transition depopulating the 1.15(4)-ms isomer. This observation is supported by the presence of an intense 169-keV peak in Fig. 3(a). If the electrons generating the 169-keV peak originated from K-shell conversion, a corresponding γ-ray peak should be visible in Fig. 5; however, no such peak has been observed. The 444-keV transition energy equals the sum of the 209- and 235-keV transition energies, and, therefore, the transition is set to proceed alongside the 209- and 235-keV transitions. Based on similar cases in the odd-mass bismuth isotopes [41], we propose that the 1.15(4)-ms isomer de-excites to the $9/2^-$ ground state via a cascade consisting of an $M2$ transition and two $M1$ transitions with energies of 209 and 235 keV, respectively. The 209-keV transition is also observed in the prompt γ-ray data; therefore, it is set to populate the ground state. The suggested structure of the cascade is presented in Band 3 of Fig. 6.

GEANT4 [42] simulations were performed to reproduce the conversion-electron and γ-ray spectrum of the de-excitation of the $1/2^+$ state with the decay characteristics discussed above; see Fig. 7. As a test, the simulations reproduced the calibration spectra in Figs. 3(b)–3(d) successfully. The results from the simulations support our interpretation of the de-excitation path of the $1/2^+$ isomer, with a transition energy of 165(5) keV for the depopulating $M2$ transition and a 35(10)% branching ratio for the 444-keV $E2$ transition. Figure 7(a) presents the scenario discussed above. As a comparison, the above-discussed scenario, without the parallel $E2$ transition, was simulated; see Fig. 7(b). In this scenario, 169-keV peak is clearly not as enhanced as in Figs. 7(a) and 3(a). To verify these results, spectra were generated for a scenario where the $1/2^+$ state is assumed to de-excite by a 235-keV $E3$ transition (100% branching) to the $7/2^-$ state. This result, presented in Fig. 7(c), clearly does not resemble the experimental results. A transition strength of $3.5(2)\times10^{-4}$ W.u. was obtained for the 165-keV $M2$ transition, by assuming a 100% branching ratio. This result agrees well with the value of $9.96(14)\times10^{-4}$ W.u. for the corresponding transition in ^{205}Bi [41]. There is a possibility for a ~400-keV $E3$ transition to occur between the $1/2^+$ state and the $7/2^-$ state (see Fig. 6). With a transition strength as for similar transitions in neutron-deficient odd-mass thallium [36,43], bismuth [44], and astatine [44] nuclei, a branching ratio of 5–40% can be estimated for this competing transition. However, the setup was not sensitive enough to resolve the possible $E3$ branch.

Figure 8(a) presents the energy spectrum of prompt γ rays associated with any fusion-evaporation recoil detected in the DSSD. It is evident in the figure that the dominant fusion-evaporation products are ^{205}Fr (peaks denoted by circles) and

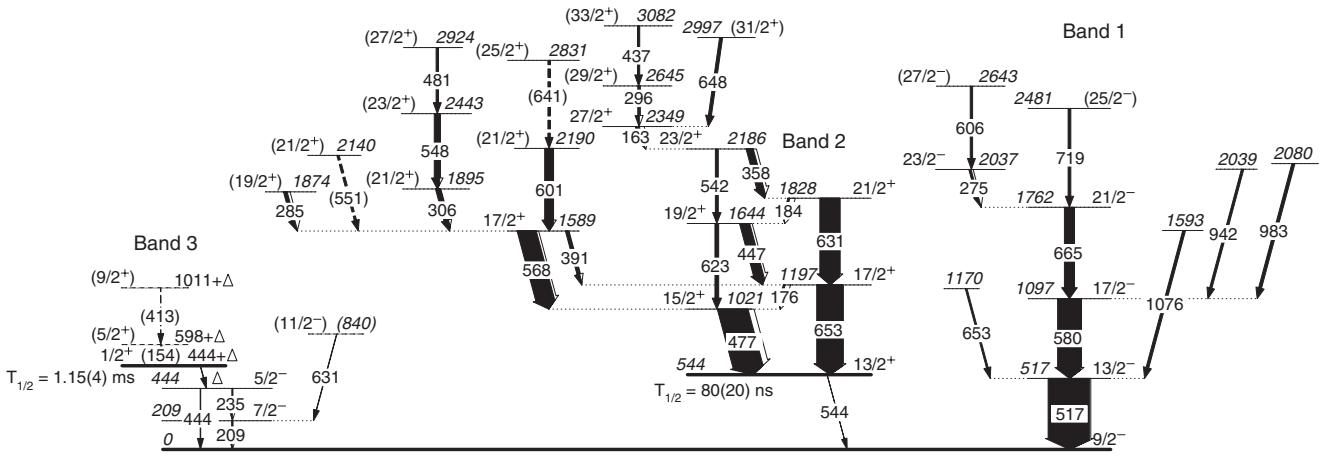

FIG. 6. The proposed level scheme. The intensity of the 544-keV isomeric transition and transitions associated with the $1/2^+$ isomer are not to scale. $\Delta = 165(5)$ keV; see text for details.

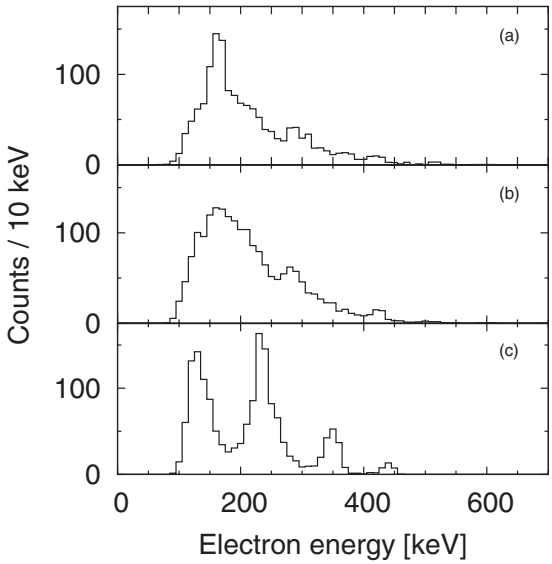

FIG. 7. Simulated electron spectra for three different scenarios in the de-excitation of the $1/2^+$ isomer. (a) The scenario of a 165(5)-keV $M2$ transition followed by a 235-keV and a 209-keV $M1$ transition, with a 35(10)% branching to a parallel 444-keV $E2$ transition. (b) The same scenario without the parallel $E2$ transition. (c) A scenario with the isomer depopulated by a 235-keV $E3$ transition followed by a 209-keV $M1$ transition. See text for further details.

^{205}Rn (peaks denoted by diamonds). The events belonging to ^{205}Rn are eliminated when tagging with the ^{205}Fr α decay, as shown in Fig. 8(b). Events from the Coulomb-excited ^{169}Tm target ions still leak through despite α-decay tagging. The strongest of these peaks are denoted by open circles. The fusion-evaporation reaction also produces neutrons which excite the germanium nuclei in the HPGe detector material. The resulting γ rays cannot be completely filtered out, and, thus, two broad peaks close to 600 and 840 keV [47,48] are visible in Fig. 8 (and in the inset of Fig. 5).

Angular-distribution measurements were performed for a number of strong γ-ray transitions. The prompt γ-ray data were sorted according to the four detector rings (at angles of 158°, 134°, 108°, and 94° with respect to the beam direction) of the JUROGAM array. The relative-efficiency corrected data for each transition were studied relative to the detector angle. Legendre polynomials according to the method presented in the work by Yamazaki [49] were fitted to the data to obtain the value of the A_2 coefficient. The A_4 coefficient was set to zero as the aim was to distinguish between the possible stretched dipole and stretched $E2$ character of the transition and not to consider quadrupole mixing. The obtained values for the Legendre polynomial A_2 coefficient, where the procedure was possible, are presented in Table I, with a negative value usually presenting a stretched dipole transition and a positive value a stretched $E2$ transition. The level scheme resulting from the analysis is presented in Fig. 6 and further details for each transition are presented in Table I.

Figure 8(c) presents the spectrum of coincident γ rays obtained by setting an energy gate on the 517-keV peak, which is the strongest of the γ-ray transitions associated with the

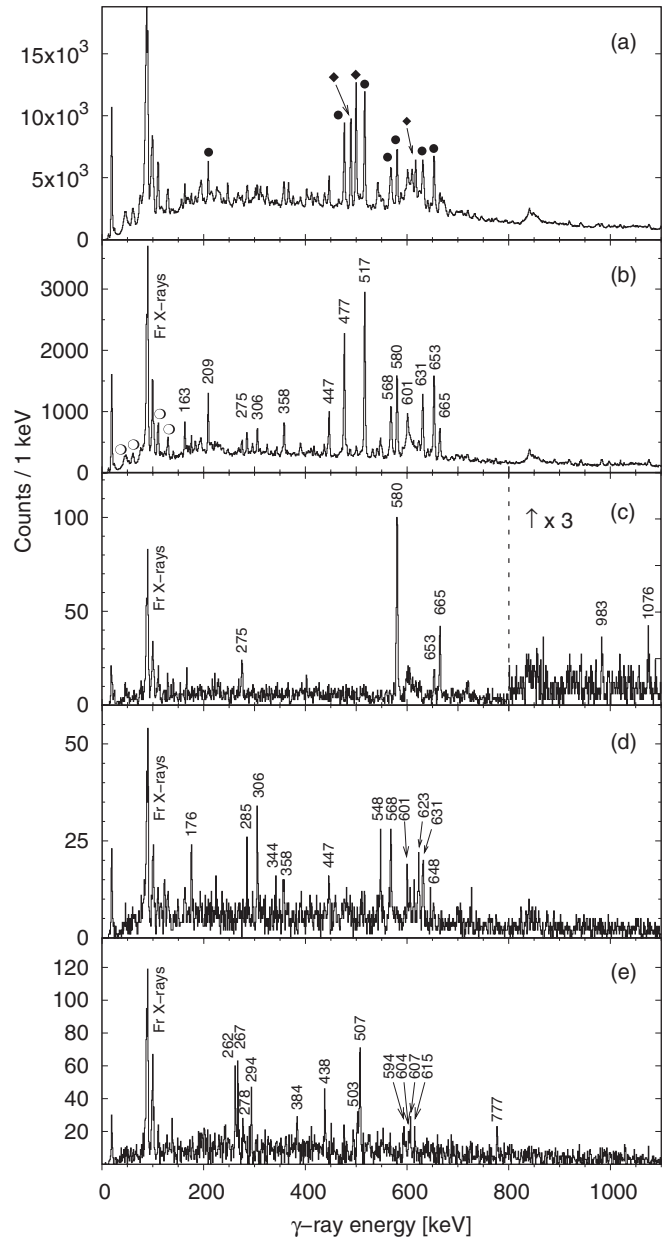

FIG. 8. (a) Spectrum of singles prompt γ rays obtained by requiring a recoil implantation in the DSSD. Peaks belonging to ^{205}Fr are indicated by circles and those belonging to ^{205}Rn [45] by diamonds. (b) Spectrum of singles prompt γ rays tagged with the α decay of ^{205}Fr. Transitions belonging to ^{169}Tm [46] are indicated by open circles. [(c) and (d)] Spectra of transitions in coincidence with the 517- and the 477-keV transition, respectively. The two spectra include γ rays tagged with escaped α particles. The intensity scale of the high-energy end of panel (c) has been expanded threefold. (e) Spectrum of prompt singles γ rays tagged with the α decay of ^{206}Fr. Note the broad peaks close to 600 and 840 keV, visible in each panel, originated from the $(n, n'\gamma)$ reaction in the detector material.

^{205}Fr recoils. The spectrum shows strong transitions at 580 and 665 keV. All three transitions have positive A_2 values (see Table I) and are, thus, assigned an $E2$ multipolarity. This sequence of transitions is placed on top of the $9/2^-$ ground state, and it forms a regular level pattern up to a $21/2^-$ state

TABLE I. The energies and relative γ-ray intensities of transitions assigned to ^{205}Fr. Results for A_2 coefficients from angular-distribution measurements are included where they could be obtained. The transitions associated with Band 3 are placed separately at the bottom of the table.

E_γ (keV)	I_γ(%)	I_i^π	I_f^π	A_2	E_γ (keV)	I_γ(%)	I_i^π	I_f^π	A_2
140.2(1)	3.8(6)				568.5(1)	45(2)	$17/2^+$	$15/2^+$	−0.28(16)
162.9(1)	9.5(5)	$27/2^+$	$23/2^+$	0.23(9)	580.5(1)	56(2)	$17/2^-$	$13/2^-$	0.28(4)
166.8(2)	3.5(5)				601.3(1)	21(2)	$(21/2^+)$	$17/2^+$	
170.9(2)	1.9(4)				605.8(3)	5.6(11)	$(27/2^-)$	$23/2^-$	
175.8(1)	4.2(4)	$17/2^+$	$15/2^+$		623.5(2)	8.8(9)	$19/2^+$	$15/2^+$	
183.6(2)	4.8(6)	$21/2^+$	$19/2^+$		630.9(1)[a]	48(2)	$21/2^+$	$17/2^+$	0.24(3)
191.2(3)	3.7(6)				640.9(2)	5.8(9)	$(25/2^+)$	$(21/2^+)$	
194.5(2)	6.3(6)				648.2(2)	7.3(9)	$(31/2^+)$	$27/2^+$	
275.3(1)	5.4(5)	$23/2^-$	$21/2^-$	−0.51(13)	653.2(1)[a]	63(2)	$17/2^+$	$13/2^+$	0.21(5)
285.0(1)	8.7(5)	$(19/2^+)$	$17/2^+$		664.6(1)	24(1)	$21/2^-$	$17/2^-$	0.29(7)
296.0(2)	3.7(5)	$(29/2^+)$	$27/2^+$		675.7(5)	3.5(10)			
305.6(1)	11(1)	$(21/2^+)$	$17/2^+$		688.4(5)	3.5(8)			
324.9(2)	3.5(5)				697.2(4)	5.2(11)			
343.6(2)	2.4(4)				701.4(3)	4.9(11)			
358.2(6)	17(1)	$23/2^+$	$21/2^+$	−0.29(11)	707.6(3)	5.5(10)			
390.6(1)	6.4(5)	$17/2^+$	$17/2^+$		714.2(4)	3.8(8)			
411.4(2)	3.4(5)				719.2(2)	6.5(8)	$(25/2^-)$	$21/2^-$	
417.0(2)	3.3(5)				774.6(2)	3.7(6)			
437.3(1)	5.1(5)	$(33/2^+)$	$(29/2^+)$	0.43(17)	840.8(3)	7(4)			
446.6(1)	24(1)	$19/2^+$	$17/2^+$		848.3(6)	7.0(15)			
472.4(2)	4.1(6)				857.6(8)	4.0(15)			
476.6(2)	72(2)	$15/2^+$	$13/2^+$	−0.17(4)	890.3(3)	3.7(7)			
481.2(2)	5.6(6)	$(27/2^+)$	$(23/2^+)$		919.1(2)	5.5(7)			
516.8(2)	100(2)	$13/2^-$	$9/2^-$	0.25(1)	942.4(2)	5.5(7)	—	$17/2^-$	
532.4(2)	6.0(8)				983.2(2)	7.1(7)	—	$17/2^-$	
541.4(2)	6.8(10)	$23/2^+$	$19/2^+$	0.6(3)	997.7(3)	4.5(7)			
544(1)[b]		$13/2^+$	$9/2^-$		1020.0(4)	3.0(7)			
547.5(1)	13(2)	$(23/2^+)$	$(21/2^+)$	−0.48(4)	1076.0(2)	6.5(8)	—	$13/2^-$	
550.6(3)	5.4(9)	$(21/2^+)$	$17/2^+$						
154.3(5)		$(5/2^+)$	$1/2^+$		235(1)		$5/2^-$	$7/2^-$	
165(5)[c]		$1/2^+$	$5/2^-$		413.1(5)		$(9/2^+)$	$(5/2^+)$	
209(1)[d]	19(1)	$7/2^-$	$9/2^-$		444(2)		$5/2^-$	$9/2^-$	

[a]The peak is a doublet.
[b]The transition is isomeric.
[c]The γ ray was not observed, see text for details.
[d]The transition is also visible in Fig. 8(b).

(see Band 1 in Fig. 6). A 275-keV stretched dipole (presumably of $M1$ multipolarity) transition is in coincidence with each of these transitions and is, therefore, assigned to depopulate a $23/2^-$ state. Figure 8(c) shows a 653-keV transition in clear coincidence with the 517-keV transition but not with the other transitions in Band 1. Therefore, it is set to precede the 517-keV transition. It is evident that the 653-keV peak must be a doublet by comparing its intensity with the intensity of the 580-keV transition between Figs. 8(b) and 8(c). A 606-keV transition was observed to populate the $23/2^-$ state. High-energy transitions (with energies of 719, 942, 983, and 1076 keV) were observed in coincidence with the low-lying ground-state band transitions.

It is evident that some of the most intense peaks in Fig. 8(b) are not visible in Fig. 8(c), implying that the transitions in Fig. 8(b) can be divided into two dominating structures. Figures 8(c) and 8(d) indicate that the intense 477-keV transition in Fig. 8(b) is not in coincidence with the 517-keV transition or with any of the other transitions in Band 1. This $M1$ transition is assumed to populate the $13/2^+$ state. Coincidence and energy relations produce a strongly coupled band, up to a spin and parity of $23/2^+$, including γ-ray transitions with energies of 176, 184, 358, 447, 477, 542, 623, 631, and 653 keV. Angular distribution measurements support the multipolarity assignments for several of these transitions. This sequence is indicated as Band 2 in Fig. 6.

Figure 6 presents several transitions feeding into Band 2, of which the most intense is the 568-keV transition. It is also one of the most intense peaks in Fig. 8(d) produced by setting a gate on the 477-keV transition. It is not in coincidence with the other transitions in Band 2 and is, therefore, set to populate the $15/2^+$ state. Results from angular-distribution measurements

provide a stretched dipole character for the transition, and it is, thus, placed to depopulate a $17/2^+$ state. A weaker 391-keV transition can be assigned to depopulate this state to the $17/2^+$ state in Band 2. A γ-ray peak at 601-keV is the strongest peak visible in the spectrum gated on the 568-keV transition.

A 163-keV $E2$ transition is clearly visible when setting an energy gate on the 358-keV transition. This transition is, furthermore, in coincidence with the 447-, 631-, and 653-keV transitions. The transition is placed to depopulate a $27/2^+$ state to the $23/2^+$ state in Band 2. Similarly, the rest of the transitions in these cascades are placed based on coincidence studies.

The inset of Fig. 5 presents prompt γ rays associated with the $1/2^+$ isomer. Lack of statistics did not allow for an adequate γ-γ coincidence analysis, although some weak evidence for coincidences between the 154- and 413-keV transitions was found. The ordering of the transitions is purely based on their intensities. The strength of the x-ray peak suggests an $E2$ multipolarity for the 154-keV transition. There is, however, a weak γ-ray peak close to an energy of 200 keV. If a considerable amount of the x-ray intensity originates from the internal conversion of this peak, the total internal conversion coefficient of the 154-keV transition will be lower and the multipolarity could approach the value of an $E1$ transition. The spin and parity assignments of the states remain, therefore, tentative.

The γ-ray transitions reported by Hartley *et al.* [15] were not observed in the present work among the transitions associated with ^{205}Fr. In the previous work RDT-type tagging methods were not used; instead, the identification of the studied isotopes relied on excitation-function analysis. We have found that the γ-ray transitions identified in the previous study actually belong to the neighboring isotope ^{206}Fr as shown in Fig. 8(e), where observed transitions include the 503-, 507-, and 777-keV transitions previously reported as belonging to ^{205}Fr. The 384-keV transition reported by Hartley *et al.* to belong to ^{206}Fr is clearly visible in this spectrum, with the 262-, 267-, 278-, and 294-keV transitions reported as part of the shears band. Furthermore, the 438-keV transition and the group of transitions close to 600-keV have not been previously reported. There are three α-decaying states in ^{206}Fr [38]; unfortunately, the lack of statistics in the present work and the overlap of the α-decay energies prevent us from associating the above-mentioned γ-ray transitions with the corresponding α-decaying state.

IV. DISCUSSION

The level scheme obtained for ^{205}Fr, shown in Fig. 6, presents separate positive-parity and negative-parity structures. This scheme differs from what has earlier been found for heavier francium nuclei [13,14], where the positive-parity states de-excite toward the ground state through high-lying negative-parity states. The origin of this change is in the lowering of the $13/2^+$ state, which de-excites to the ground state. A similar transformation has been observed in the odd-mass astatine nuclei when comparing ^{199}At [37] with heavier astatine isotopes (see Refs. [21,50] and references therein).

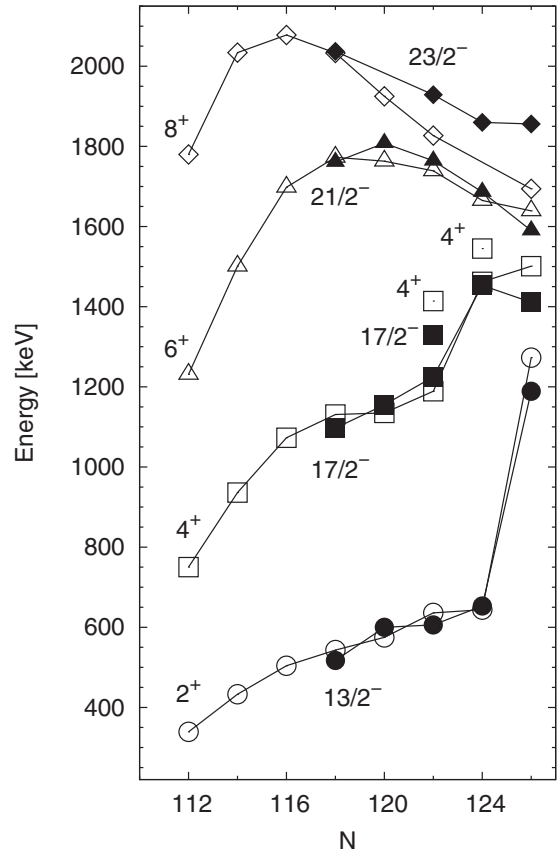

FIG. 9. Level energies of negative-parity states in odd-mass francium nuclei compared with yrast and near-yrast positive-parity states in their even-mass radon isotones. ^{205}Fr has a neutron number of 118. For the radon data, denoted by open symbols, see the studies in Refs. [5,8–10,51]. The data for the heavier francium nuclei are taken from the studies in Refs. [13–15]. The lines connect yrast states without specifying the configuration of the states.

Figure 9 presents energy systematics of negative-parity states in odd-mass francium nuclei compared with yrast levels in their radon isotones. The increasing number of valence neutron holes lowers the level energies when moving away from the closed neutron shell. The first sign of the effect is visible in the drastic drop of the 2^+ state in ^{210}Rn, caused by the opening of the first neutron shell. While the corresponding state in ^{212}Rn is still purely a $(\pi h_{9/2})^4$ state, the neutron holes generate components in the wave function of the 2^+ state bringing the state down in energy. This scheme is followed by the francium isotones, with a clear analogy visible for the $13/2^-$ state. The same effect appears in the radon 4^+ states at ^{208}Rn, where both the proton state and the yrast neutron state have been observed. The nonyrast proton state is still known in ^{206}Rn, but as the neutron states decrease in energy, the proton state is nonyrast and is not observed in the lighter even-mass radon isotopes. Again, the $17/2^-$ states in the francium isotones show a similar behavior with a change between proton and neutron-hole configuration in ^{209}Fr. Although collectivity increases with each new neutron

hole, the level spacing between the 2^+ and 4^+ states in the radon nuclei indicates that no sign of the proton intruder configuration, visible in ^{198}Rn [10], is yet to be expected this far from the neutron mid-shell in the francium nuclei. Further up in energy, the 6^+ states show signs of neutron-hole configurations in ^{202}Rn, where a down bend in the energy curve is visible. Francium systematics do not reach this far yet, and the $21/2^-$ state in ^{205}Fr could still originate from the $(\pi h_{9/2})^3$ configuration. Furthermore, the $23/2^-$ state could originate from the $(\pi h_{9/2})^2 f_{7/2}$ configuration.

Band 1 includes states feeding into the cascade mentioned above. A $(25/2^-)$ state has been observed at a level energy of 2481 keV and can be interpreted as originating from the maximum alignment of the five $h_{9/2}$ protons. This state is expected to lie approximately 750 keV above the $21/2^-$ state in odd-mass francium nuclei [13]. It has not been observed in ^{213}Fr and ^{211}Fr [14], but it has been observed in ^{209}Fr [13] at a level energy of 2559 keV (that is 795 keV above the $21/2^-$ state). The level-energy difference of 719 keV between the $(25/2^-)$ and $21/2^-$ states in ^{205}Fr agrees well, therefore, with these observations. The $(27/2^-)$ state in ^{205}Fr, at a level energy of 2643 keV, is observed to de-excite to the $23/2^-$ state discussed earlier. It is interpreted as originating from the $\pi(h_{9/2})^4 f_{7/2}$ [or the $\pi(h_{9/2})^2 f_{7/2} \otimes 2^+$] configuration. Similar states have earlier been observed in ^{209}Fr and in ^{213}Fr at level energies of 2599 and 2740 keV, respectively.

Strongly coupled bands have been observed on top of the $13/2^+$ state in ^{197}At and ^{199}At, indicating an oblate deformation for the $13/2^+$ state [37]. A similar, but slightly weaker, coupling is observed for the band built on top of the $13/2^+$ state in the present work (Band 2), indicating that the $13/2^+$ state in ^{205}Fr originates from the odd proton in the $13/2^+[606]$ Nilsson state. Plots of kinematic moments of inertia $\mathcal{J}^{(1)}$, extracted from the level energies, for Band 2 in ^{205}Fr compared with similar bands in neighboring nuclei are presented in Fig. 10. The result for ^{205}Fr follows the same, quite linear, behavior as the other nuclei, with collective characteristics similar to those of ^{199}At. The high-spin point, with a $\mathcal{J}^{(1)}$ value close to 40 $\hbar^2$ MeV^{-1}, shows a clear deviation from the smooth behavior. This deviation may suggest that the $23/2^+$ state is no longer part of the structure of Band 2.

A group of positive-parity states, identified in the odd-mass bismuth ($A > 191$), astatine ($A > 199$), and francium ($A > 209$) nuclei, are formed by coupling the odd $h_{9/2}$ proton to the negative-parity states of the corresponding even-even core nucleus. For example, the negative-parity states 5^- $[(\nu f_{5/2})^{-1}(\nu i_{13/2})^{-1};(\nu p_{3/2})^{-1}(\nu i_{13/2})^{-1}]$ at 1909 keV, 7^- $[(\nu f_{5/2})^{-1}(\nu i_{13/2})^{-1};(\nu p_{3/2})^{-1}(\nu i_{13/2})^{-1};(\nu p_{1/2})^{-1}(\nu i_{13/2})^{-1}]$ at 2154 keV, 9^- $[(\nu f_{5/2})^{-1}(\nu i_{13/2})^{-1}]$ at 2183 keV, and 6^- (similar configuration as the 5^- or 7^- state) at 2257 keV in ^{200}Pb [53], which is the isotone of ^{205}Fr, are formed by the valence neutron pairs. It is worth noting that these core states are very stable in level energy against changing neutron number; see, for instance, the studies (and references therein) for systematics in lead [54] and polonium [55] nuclei. Similar negative-parity states are expected to exist in ^{204}Rn, although a complete set of them has not yet been observed [9]. When these states are coupled to the odd $h_{9/2}$ proton, the favored J_{MAX}-1 $17/2^+$, $21/2^+$, $25/2^+$, and $19/2^+$ states are formed. Additionally, a 10^- $(f_{7/2}i_{13/2})$ state is present in the ^{204}Rn isotone at 2462 keV [9]. Coupling the odd $h_{9/2}$ proton to this 10^- state yields the J_{MAX} state $29/2^+$. Similarly, the 11^- $(h_{9/2}i_{13/2})$ state in ^{204}Rn at 2597 keV yields a J_{MAX} state $29/2^+$ in ^{205}Fr when coupled with the odd $h_{9/2}$ proton.

Positive-parity states based on the configurations discussed above can be associated with levels in ^{205}Fr observed in the present work. The $17/2^+$ state at 1589 keV is interpreted to have the configuration $\pi h_{9/2} \otimes 5^-$. A $17/2^+$ state lies at 1748 keV in the isotone ^{201}Bi. Further, in the isotone ^{203}At, two $17/2^+$ states have been observed at level energies of 1633 and 1696 keV, respectively. Both states have an $E2$ branch to the $13/2^+$ state and an $M1$ branch to the $15/2^+$ state. In ^{205}Fr the $17/2^+$ state feeds the $15/2^+$ state in Band 2. The $(21/2^+)$ (at 1895 keV) and $(19/2^+)$ (at 1874 keV) states are interpreted to have the configurations $\pi h_{9/2} \otimes 7^-$ or $\pi h_{9/2} \otimes 6^-$. Similarly, the $23/2^+$ state at 2186 keV could have the configuration $\pi h_{9/2} \otimes 7^-$ with maximum alignment, although the transition to the $21/2^+$ state is missing. The $27/2^+$ state at 2349 keV is suggested to have the configuration $\pi h_{9/2} \otimes 10^-$. There is no good candidate for the $25/2^+$ state ($\pi h_{9/2} \otimes 9^-$). If it is isomeric as in ^{209}Fr [13], it will remain unobserved in RDT experiments such as the present one. Finally, the $(29/2^+)$ J_{MAX} state at 2645 keV could originate from the $\pi h_{9/2} \otimes 11^-$ configuration.

The $1/2^+$ state has been identified and assigned as originating from a proton-hole in the $s_{1/2}$ shell. The corresponding state has been observed in odd-mass bismuth isotopes. In ^{205}Bi this $1/2^+$ state de-excites by a hindered $M2$ transition to a $5/2^-$ state [41]. In ^{203}Bi a competing $E3$ transition to a $7/2^-$ state has additionally been observed [41]. In ^{201}Bi and ^{199}Bi these two states lie above the $1/2^+$ state, and the $1/2^+$ state (with a half-life of tens of minutes) decays mainly by electron capture but also de-excites by a strongly hindered $M4$ transition to the $9/2^-$ ground state. In the present work, the $5/2^-$ state is assigned to belong to the $\pi h_{9/2} \otimes 2^+$ multiplet as in the isotopes ^{199}Bi to ^{205}Bi, but, unlike in the bismuth nuclei, the $7/2^-$ level

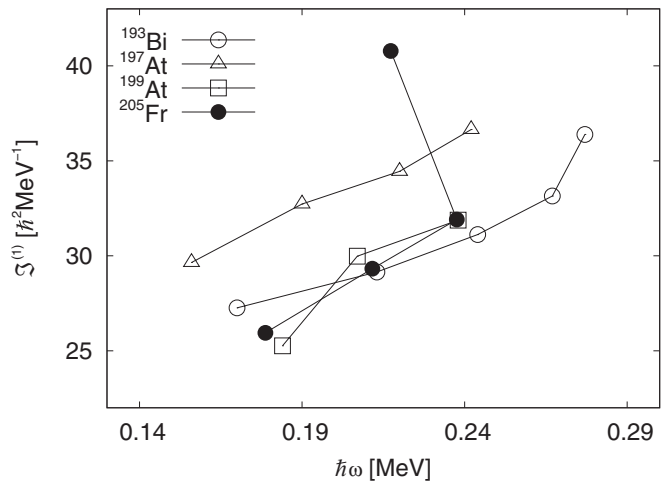

FIG. 10. Experimental kinematic moments of inertia of the rotational band feeding the $13/2^+$ isomer in ^{205}Fr compared with neighboring oblate deformed nuclei. The data for the astatine nuclei are taken from Ref. [37] and the bismuth data from Ref. [52].

TABLE II. The proposed configurations for some of the states in ^{205}Fr.

	E_{state} (keV)	Configuration
$9/2^-$	0	$\pi h_{9/2} \otimes 0^+$
$13/2^-$	517	$\pi h_{9/2} \otimes 2^+$
$17/2^-$	1097	$\pi h_{9/2} \otimes 4^+$
$21/2^-$	1762	$\pi h_{9/2} \otimes 6^+$
$23/2^-$	2037	$\pi (h_{9/2})^2 f_{7/2}$
$25/2^-$	2481	$\pi (h_{9/2})^5_{\text{MAX}}$ or $\pi (h_{9/2})^3 \otimes 2^+$
$27/2^-$	2643	$\pi (h_{9/2})^4 f_{7/2}$ or $\pi (h_{9/2})^2 f_{7/2} \otimes 2^+$
$13/2^+$	544	$\pi i_{13/2}$
$17/2^+$	1589	$\pi h_{9/2} \otimes 5^-$
$23/2^+$	2186	$\pi h_{9/2} \otimes 7^-$
$27/2^+$	2349	$\pi h_{9/2} \otimes 10^-$
$29/2^+$	2645	$\pi h_{9/2} \otimes 11^-$
$1/2^+$	$444 + \Delta$	$\pi (s_{1/2})^{-1}$
$7/2^-$	209	$\pi f_{7/2}$
$5/2^-$	444	$\pi h_{9/2} \otimes 2^+$

lies further away from the $5/2^-$ state, which indicates that it is not part of the multiplet. It is, therefore, assumed to originate from the odd proton on the $f_{7/2}$ shell as in the lighter bismuth and astatine nuclei [19,22]. Similarly to the behavior in the bismuth nuclei, the $1/2^+$ state in ^{205}Fr continues the rising trend in level energy when approaching the closed neutron shell. This is a characteristic feature of the intruder states involving proton excitations across the $Z = 82$ shell gap.

Finally, no additional higher-spin isomers, as reported in the heavier odd-mass francium nuclei, were observed in the present study. If such isomers exist in ^{205}Fr, they would need to be as fast as to decay inside the RITU separator but as slow as not to be seen by the JUROGAM array (Table II).

V. CONCLUSIONS

The nucleus ^{205}Fr has been studied using both in-beam γ-ray and delayed γ-ray and electron spectroscopy. We present results of the de-excitation of the $13/2^+$ isomer, with a weakly deformed band built on top of the isomer. A series of transitions to the $9/2^-$ ground state have also been observed. This result indicates that the ground-state band is still dominated by spherical structures in ^{205}Fr and pushes the onset of ground-state deformation in francium nuclei further toward the neutron mid-shell. Using highly selective electron-γ coincidence methods, the $1/2^+$ isomer was observed and it continues the tendency of a rising level energy, when approaching the closed neutron shell, as expected when comparing with odd-mass bismuth isotopes. The systematic study of the odd-mass francium isotopes would highly benefit from a deeper examination of the properties of ^{207}Fr. Certainly a continued, although challenging, search toward the proton drip line in both radon and francium nuclei would present data of high interest.

ACKNOWLEDGMENTS

This work has been supported through EURONS (European Commission contract no. RII3-CT-2004-506065) and by the Academy of Finland under the Finnish Centre of Excellence Programme 2006-2011 (Nuclear and Accelerator Based Physics contract no. 213503). The authors also thank the UK/France (STFC/IN2P3) detector Loan Pool and GAMMAPOOL European Spectroscopy Resource for the loan of the detectors for the JUROGAM array. Support has also been provided by the UK Engineering and Physical Sciences Research Council. U.J. acknowledges support from the Finnish Academy of Science and Letters; Vilho, Yrjö and Kalle Väisälä Foundation.

[1] R. Julin, K. Helariutta, and M. Muikku, J. Phys. G **27**, R109 (2001).
[2] A. M. Oros, K. Heyde, C. De Coster, B. Decroix, R. Wyss, B. R. Barrett, and P. Navratil, Nucl. Phys. A **645**, 107 (1999).
[3] K. Helariutta *et al.*, Eur. Phys. J. A **6**, 289 (1999).
[4] T. E. Cocolios *et al.*, Phys. Rev. Lett. **106**, 052503 (2011).
[5] G. D. Dracoulis, G. J. Lane, A. P. Byrne, P. M. Davidson, T. Kibédi, P. H. Nieminen, H. Watanabe, A. N. Wilson, H. L. Liu, and F. R. Xu, Phys. Rev. C **80**, 054320 (2009).
[6] A. R. Poletti, A. P. Byrne, G. D. Dracoulis, T. Kibédi, and P. M. Davidson, Nucl. Phys. A **756**, 83 (2005).
[7] W. J. Triggs, A. R. Poletti, G. D. Dracoulis, C. Fahlander, and A. P. Byrne, Nucl. Phys. A **395**, 274 (1983).
[8] D. Horn, C. Baktash, and C. J. Lister, Phys. Rev. C **24**, 2136 (1981).
[9] D. J. Dobson *et al.*, Phys. Rev. C **66**, 064321 (2002).
[10] R. B. E. Taylor *et al.*, Phys. Rev. C **59**, 673 (1999).
[11] A. N. Andreyev *et al.*, Phys. Rev. C **74**, 064303 (2006).
[12] H. Kettunen *et al.*, Phys. Rev. C **63**, 044315 (2001).
[13] G. D. Dracoulis, P. M. Davidson, G. J. Lane, A. P. Byrne, T. Kibédi, P. Nieminen, H. Watanabe, and A. N. Wilson, Phys. Rev. C **79**, 054313 (2009).
[14] A. P. Byrne, G. D. Dracoulis, C. Fahlander, H. Hubel, A. R. Poletti, A. E. Stuchbery, J. Gerl, R. F. Davie, and S. J. Poletti, Nucl. Phys. A **448**, 137 (1986).
[15] D. J. Hartley *et al.*, Phys. Rev. C **78**, 054319 (2008).
[16] R. A. Braga, W. R. Western, J. L. Wood, R. W. Fink, R. Stone, C. R. Bingham, and L. L. Riedinger, Nucl. Phys. A **349**, 61 (1980).
[17] A. N. Andreyev *et al.*, Phys. Rev. C **69**, 054308 (2004).
[18] K. Andgren *et al.*, Phys. Rev. C **78**, 044328 (2008).
[19] H. Kettunen *et al.*, Eur. Phys. J. A **16**, 457 (2003).
[20] J. Uusitalo *et al.*, Phys. Rev. C **71**, 024306 (2005).
[21] K. Dybdal, T. Chapuran, D. B. Fossan, W. F. Piel Jr., D. Horn, and E. K. Warburton, Phys. Rev. C **28**, 1171 (1983).
[22] H. Kettunen *et al.*, Eur. Phys. J. A **17**, 537 (2003).
[23] C. W. Beausang *et al.*, Nucl. Instrum. Methods A **313**, 37 (1992).
[24] C. Rossi Alvarez, Nucl. Phys. News **3**, 10 (1993).
[25] M. Leino *et al.*, Nucl. Instrum. Methods B **99**, 653 (1995).
[26] R. D. Page *et al.*, Nucl. Instrum. Methods B **204**, 634 (2003).
[27] I. H. Lazarus *et al.*, IEEE Trans. Nucl. Sci. **48**, 567 (2001).
[28] E. S. Paul *et al.*, Phys. Rev. C **51**, 78 (1995).
[29] P. Rahkila, Nucl. Instrum. Methods A **595**, 637 (2008).
[30] D. C. Radford, Nucl. Instrum. Methods A **361**, 297 (1995).

[31] D. C. Radford, Nucl. Instrum. Methods A **361**, 306 (1995).
[32] A. Y. Deo *et al.*, Phys. Rev. C **81**, 024322 (2010).
[33] H. De Witte *et al.*, Eur. Phys. J. A **23**, 243 (2005).
[34] A. N. Andreyev *et al.*, Nucl. Instrum. Methods A **533**, 422 (2004).
[35] T. Kibédi, T. W. Burrows, M. B. Trzhaskovskaya, P. M. Davidson, and C. W. Nestor Jr., Nucl. Instrum. Methods A **589**, 202 (2008).
[36] F. G. Kondev, Nucl. Data Sheets **108**, 365 (2007).
[37] U. Jakobsson *et al.*, Phys. Rev. C **82**, 044302 (2010).
[38] M. Huyse, P. Decrock, P. Dendooven, G. Reusen, P. Van Duppen, and J. Wauters, Phys. Rev. C **46**, 1209 (1992).
[39] P. Van Duppen, E. Coenen, K. Deneffe, M. Huyse, and J. L. Wood, Phys. Rev. C **35**, 1861 (1987).
[40] K.-H. Schmidt, Eur. Phys. J. A **8**, 141 (2000).
[41] T. Lönnroth, Z. Phys. A **307**, 175 (1982).
[42] S. Agostinelli *et al.*, Nucl. Instrum. Methods A **506**, 250 (2003).
[43] B. Singh, Nucl. Data Sheets **108**, 79 (2007).
[44] M. Nyman *et al.* (submitted to Phys. Rev. C).
[45] J. R. Novak *et al.*, Phys. Rev. C **59**, R2989 (1999).
[46] C. M. Baglin, Nucl. Data Sheets **109**, 2033 (2008).
[47] B. Singh and A. Farhan, Nucl. Data Sheets **107**, 1923 (2006).
[48] D. Abriola and A. A. Sonzogni, Nucl. Data Sheets **111**, 1 (2010).
[49] T. Yamazaki, Nucl. Data, Sect. A **3**, 1 (1967).
[50] R. F. Davie, A. R. Poletti, G. D. Dracoulis, A. P. Byrne, and C. Fahlander, Nucl. Phys. A **430**, 454 (1984).
[51] A. R. Poletti, T. P. Sjoreen, D. B. Fossan, U. Garg, A. Neskakis, and E. K. Warburton, Phys. Rev. C **20**, 1768 (1979).
[52] P. Nieminen *et al.*, Phys. Rev. C **69**, 064326 (2004).
[53] F. G. Kondev and S. Lalkovski, Nucl. Data Sheets **108**, 1471 (2007).
[54] B. Fant, T. Weckström, H. C. Jain, L. O. Norlin, K.-G. Rensfelt, P. Carle, and U. Rosengård, Nucl. Phys. A **475**, 338 (1987).
[55] N. Bijnens *et al.*, Phys. Rev. C **58**, 754 (1998).